


Structural modification of UHMWPE fiber through hybridization and CNT reinforcement for ballistic applications

Hassan Mahfuz¹  | Leif A. Carlsson¹ | Oren Masory¹ | Tye Langston² | Vitor Prado Correia¹ | Tristan Irons³

¹Ocean and Mechanical Engineering Department, Florida Atlantic University, Boca Raton, Florida, USA

²Expeditionary & Maritime Systems Department, Naval Surface Warfare Center Panama City Division, Panama City, Florida, USA

³Department of Physics, Florida Atlantic University, Boca Raton, Florida, USA

Correspondence

Hassan Mahfuz, Ocean and Mechanical Engineering Department, Florida Atlantic University, Boca Raton, FL 33431, USA.
Email: hmahfuz@fau.edu

Funding information

Irregular Warfare Technical Support Directorate, Grant/Award Number: N4175619C3083

Abstract

In the construction of an armor for ballistic protection, fibers are used in the form of a laminated composite bonded to the back of the frontal ceramic layer. The composite layer dissipates energy transmitted through the ceramic layer and controls the spall. To absorb energy locally and to spread it out fast, fibers in the composite layer must have high toughness and tensile wave speed as quantified by a primary performance index called normalizing velocity. The goal of this investigation is to increase the normalizing velocity of ultra-high molecular weight (UHMWPE) fiber that is widely used in ballistic protection. The structure of UHMWPE is modified by hybridizing with nylon and reinforcing with carbon nanotubes. Fibers are extruded by melt-spinning. The concentration of nylon and nanotubes is 18 and 2 wt%, respectively. After extrusion, fibers are strain-hardened by cyclic loading to align UHMWPE molecules and nanotubes along the fiber axis. Tensile properties are determined to calculate normalizing velocity. Normalizing velocities up to 1270 m/s were obtained for the modified fiber which outperforms Spectra-2000 and Dyneema-SK75 by 44%–57%. Materials chemistry and structure of the fiber are investigated through differential scanning calorimetry (DSC), Raman Spectroscopy, and scanning electron microscope (SEM). It was observed that microdroplet formation by the nylon phase during hybridization promotes interface sliding of UHMWPE ligaments and elevates the fracture strain. Raman and SEM examination demonstrates that embedded nanotubes get aligned along the fiber axis due to strain hardening and co-continuously deform with UHMWPE sharing the load.

KEYWORDS

Ballistic fiber, nanotube reinforcement, normalizing velocity, polymer hybridization

1 | INTRODUCTION

In flexible or ceramic-based armor, fiber plays a critical role. Fibers impregnated with a light resin in multiple

layers can be pressed into a panel or attached to a ceramic layer as backing composite. Primary purpose of the backing plate is to absorb kinetic energy of the projectile through deformation of the fiber and spread it out as

quickly as possible without localization.¹ To maximize this absorption and dissipation, fiber should have high toughness and tensile wave speed. A primary performance index combining toughness and tensile wave speed is given by the normalizing velocity as defined below.²

$$\sqrt[3]{\Omega} = \left[\frac{\sigma_{\max} \varepsilon_{\max}}{2\rho} \sqrt{\frac{E}{\rho}} \right]^{\frac{1}{3}} \quad (1)$$

where σ , ε , E , and ρ are strength, fracture strain, modulus, and density of the fiber, respectively. The cubic root is to get velocity in units of m/s. The quantity $\sqrt[3]{\Omega}$ is widely known as normalizing velocity and used as a quantitative measure of fiber performance. The goal of any ballistic fiber manufacturer is to increase the normalizing velocity. A list of various commercial fibers used for ballistic application is given in a Table 1. It is observed in Table 1 that Spectra, Dyneema, and Zylon fibers all have high normalizing velocity above 800 m/s. It is noticed that Nylon has a normalizing velocity of 504 m/s and is never used in armor applications. Dyneema and Spectra are UHMWPE-based fiber and our idea in this paper is to structurally modify the polymer to increase the normalizing velocity.

A hybrid of two polymers namely, UHMWPE and nylon-6 are considered in this investigation. UHMWPE is a linear homopolymer with a large molecular weight of 3 M g/mole.³ The van der Waal bonds between UHMWPE chains are weak, but the long chain structure can transfer load efficiently if chains can be aligned with the axis of the fiber. The molecular chain of UHMWPE is flexible and allows chain folds to form a crystalline structure. The degree of crystallinity of UHMWPE is about 50%. Such long chain configurations accompanied with crystalline structure is the reason UHMWPE is used as a polymer precursor for ballistic fibers like Dyneema and Spectra demanding high modulus and strength. On the

other hand, nylon-6 has relatively low crystallinity (~35%), low modulus, and strength. Although nylon is a common fiber material, it is never used in ballistic applications. Nylon has weak interchain H-bonds, which gives rise to anisotropic sheet like structures within the crystalline phase.^{3–6} Nylon-6 can undergo large plastic deformation by crystal slip of the H-bonded sheets. The combination of two different molecular structures of UHMWPE and nylon-6 provides a synergistic advantage. Modulus and strength of Dyneema SK75 (107 GPa and 3400 MPa, respectively) are almost an order of magnitude higher than those of nylon-6 (4.14 GPa and 420 MPa, respectively). But the fracture strain of Dyneema SK75 (3.8%) is an order of magnitude lower than that of nylon (37%). Although the properties are different for the two polymers, the data provides a design window. If the two polymers can be blended as one precursor, the resulting fiber will have higher fracture strain but an intermediate modulus and strength between UHMWPE and nylon-6. Over the last several years, it has been demonstrated that dispersion of carbon nanotubes (CNT) in a polymer can increase modulus and strength significantly.^{7–9} Several other researchers also dispersed CNTs into various polymer and aligned CNTs along the length of the drawn filament.^{10–14} Alignment of CNTs in a filament may be enforced by extrusion or spinning followed by heat stretching resulting in improved mechanical properties. Unfortunately, addition of CNTs always resulted in significant reduction of fracture strain.

In recent years low density polyethylene (LDPE) and UHMWPE have been reinforced with CNTs. Our recent work revealed that in addition to CNT reinforcement, a second phase polymer may be used to increase toughness.^{15–20} If the blended polymer can be reinforced with CNTs, the modulus and strength of the hybridized fiber will increase while maintaining most of the fracture strain. This strategy of hybridization and nanotube-reinforcement was the premise of the current investigation. As-produced fibers were strain hardened to further

TABLE 1 Mechanical properties and normalizing velocities of various fibers.

Fiber	Density (ρ , kg/m ³)	Modulus (E ; GPa)	Strength (σ ; GPa)	Fracture strain (ε ; %)	Normalizing velocity ($\sqrt[3]{\Omega}$, m/s)
Nylon-66	1150	4.14	0.42	37	504
Kevlar-29	1440	74	2.9	3.4	626
Kevlar-KM2	1440	70	3.3	4.0	684
Spectra 2000	970	116	3.25	2.9	809
Dyneema SK75	970	107	3.4	3.8	887
Zylon HM	1560	270	5.8	2.5	849
Zylon AS	1540	180	508	3.5	893

align the nanotubes and to disentangle large UHMWPE molecular chains.

In our approach, the following innovative steps were implemented to increase the normalizing velocity which depends on modulus, strength, and fracture strain of the fiber. UHMWPE is first hybridized with nylon to increase fracture strain. Hybridization however reduces the modulus and strength. Hybridized polymer is then reinforced with CNT to recover lost modulus and strength. Further, composite fiber is strain hardened to increase modulus and strength by aligning UHMWPE ligaments and CNTs along the axis of the fiber. Combination of these steps resulted in fiber with enhanced normalizing velocity.

2 | MATERIALS AND METHODS

Primary materials in this investigation were UHMWPE, Nylon, and functionalized carbon nanotubes, namely, single-walled carbon nanotubes functionalized with carboxyl group (SWCNT-COOH) and single-walled carbon nanotubes functionalized with octadecylamine (SWCNT-ODA). Functionalized nanotubes were procured from Sigma Aldrich (3050 Spruce Street, St. Louis, Missouri 63,103, USA). Nylon-6 was procured from UBE Industries Ltd. (Tokyo, Japan). Both UHMWPE and Nylon-6 were obtained in powdered form. Paraffin oil was used as a solvent to prepare the mixture and was procured from Sigma Aldrich. The reason for using the two functional groups for the nanotubes was to promote dispersion by reducing the van der Waals interaction among nanotubes. SWCNT-ODA nanotubes had both carboxyl and alkane groups on the surface, and the long alkyl chain of ODA was compatible with the molecular structure of UHMWPE.²¹ Recent research indicates that these functional groups have been used to enhance mechanical properties of polyethylene.^{22,23}

Paraffin oil was used as a solvent to help disperse nanotubes, dissolve UHMWPE and nylon, and facilitate melt extrusion. In this investigation paraffin oil was not treated with any other chemical compound like CO₂ or Decalin as carried out by other researchers.^{24–26} The ratio of paraffin oil to solid (i.e., UHMWPE + nylon + SWCNT's) was optimized by several iterations of spinning and testing the fiber. The optimum ratio was 97:3 by weight. Mixing nanotubes into paraffin oil was carried out with ultrasonic cavitation for about 30 min. Once the nanotubes were dispersed, UHMWPE and nylon powders were added to the solution using a homogenizer for 10 min. The concentrations of UHMWPE, nylon and SWCNT's were 80%, 18%, and 2% by weight, respectively.

After the solution was prepared, it was fed into a laboratory mixing extruder (LME) as shown in Figure 1.

The extruder included a coaxial cylinder, a turning rotor heater, an outlet die, an orifice, a water bath, and a take-up system.³ As the solution passed through the annular zone of the extruder, it was heated to about 140°C. At this stage, the solution formed into a viscous gel which flowed into the outlet die and exited through the nozzle as a filament. The rotor and header temperature of the extruder were set at 140°C and 150°C, respectively. The speed of the turning rotor was kept low to avoid excessive shear which could lead to shear-degradation of macromolecules. After extrusion, filaments were cooled in a water bath, air-dried, and collected in a spool as shown in step (a) of Figure 1. The next step was the solvent extraction stage. Filaments from the take-up roll is transferred in smaller quantity by wrapping around a cylindrical rod and submerged for about 15 minutes into a hexane bath shown in Figure 1b. After the hexane treatment, filaments were air dried. In the final stage, dried filaments were heat-stretched in front of a heater as shown in Figure 1c. The speed of stretching was controlled by hand to produce fibers with diameters varying from 20 to 50 μm. Three categories of fiber were produced, namely, neat UHMWPE, Nanohybrid SWCNT-COOH, and Nanohybrid SWCNT-ODA.

3 | EXPERIMENTAL

After the fibers were prepared, they were tested in tension, strain hardened, and characterized through differential scanning calorimetry (DSC), Raman, and scanning electron microscope (SEM). Tensile tests and strain hardening were conducted using a Zwick-Roel materials testing machine. Details of fiber testing and strain hardening are described in Sections 3.1 and 3.2. DSC tests were performed in a TA Instruments Q10 series apparatus. Tests were run in both heating and cooling ramps at a rate of 10°C under inert atmosphere. Five grams of sample were used in each category and heating range was from 50°C to 225°C. Raman spectroscopy was carried out using a T6400 spectrometer with 514.5-nm line of argon ion laser. SEM examination of the fiber was performed using a JEOL JSF-6330F (field emission scanning electron microscope [FESEM]). To investigate alignment of nanotubes, fiber surface was prepared by ion milling to remove the polymer and expose the embedded nanotubes.

It is to note that during ballistic application fibers will be subjected to high rates of strain, and they could be tested using a split Hopkinson pressure bar (SHPB). However, we would like to mention that UHMWPE fibers have been tested at high strain rates by Russell et al.¹ It was observed that as strain rate changes from quasi-static to 10⁰ S⁻¹, strength and modulus increases

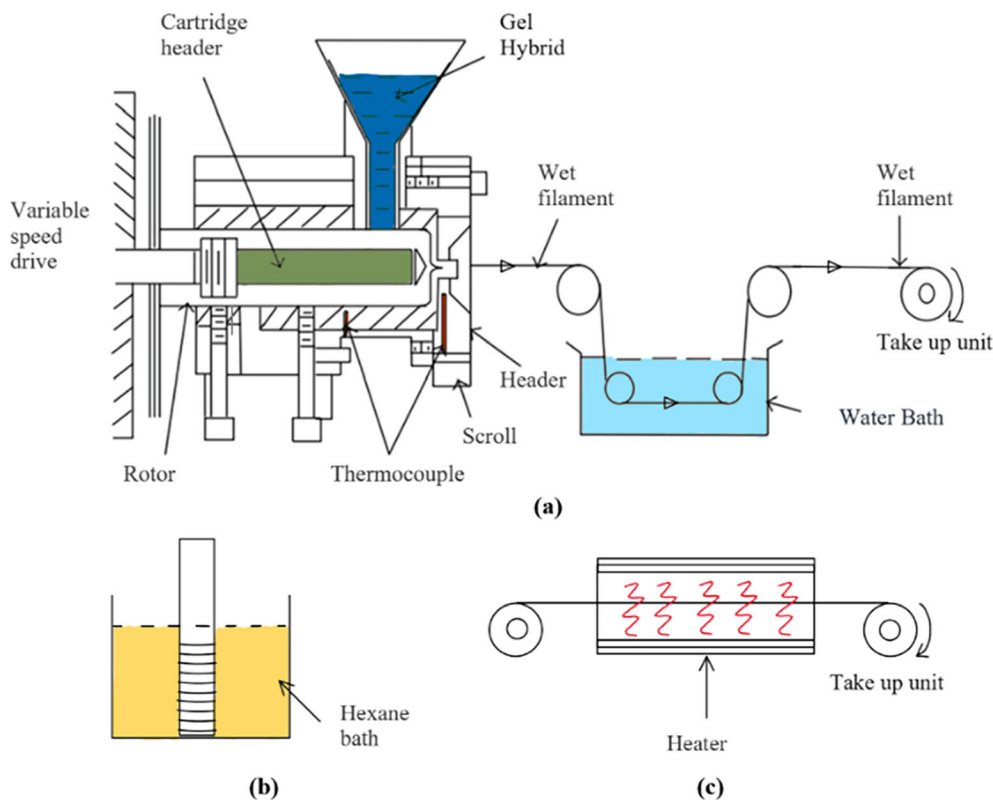


FIGURE 1 Schematic view of melt extrusion using a laboratory mixing extruder (LME). (a) Filament extrusion, water cooling, air drying and collecting in a spool, (b) solvent extraction using a hexane bath, and (c) heat stretching. [Color figure can be viewed at [wileyonlinelibrary.com](https://onlinelibrary.wiley.com/doi/10.1002/app.54035)]

by 32% and 45%, respectively. On the other hand, fracture strain reduces by 32%. If these changes in fiber property are incorporated into Equation (1), there will be a 4% change in normalizing velocity. It is also shown in reference [1] that fiber properties remain unchanged beyond 10^0 S^{-1} . This suggests that quasi-static tensile test is sufficient to determine normalizing velocity.

3.1 | Fiber tensile testing

Fiber testing was performed at quasi-static rate to determine modulus, strength, and fracture strain. Fiber testing procedure was developed using ASTM C1557-03 as a guideline.^{27–29} Two gripping methods were initially investigated: (i) glue-tab grip method and (ii) direct grip method. The glue-tab method consisted of mounting a fiber onto a rigid tab as specified in the ASTM standard using an adhesive. With glue-tab method, UHMWPE fibers failed each time near the grips rather than in the gage section. In the direct grip method, fiber was directly clamped within Poly methyl methacrylate (PMMA) blocks. When using the direct gripping method, UHMWPE fiber slipped from the PMMA clamps rendering the test invalid. Slipping occurred since the fiber diameter was low and strength was high. However, wrapping the fiber around grooved discs (Figure 2) made from polylactic acid (PLA) and then gripping the discs within the PMMA clamps was successful. Failure of the fiber

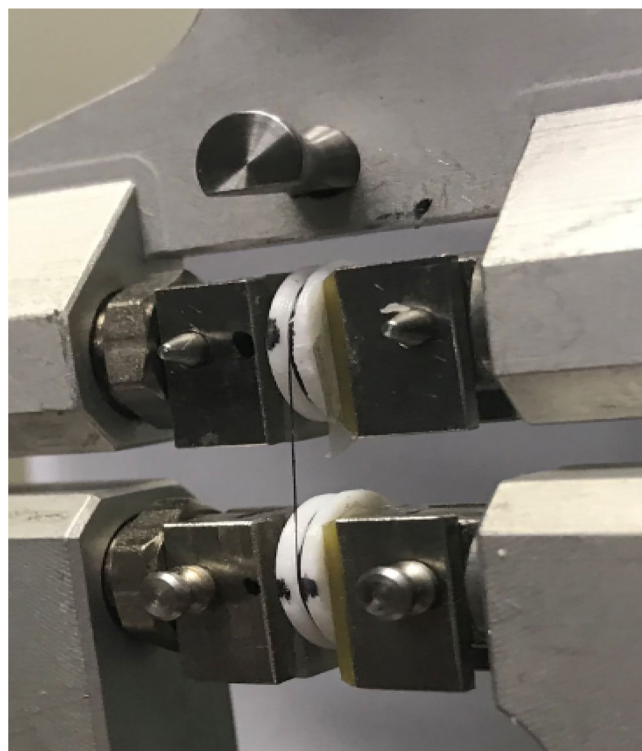


FIGURE 2 Fiber tests with grooved poly(lactic acid) (PLA) discs. [Color figure can be viewed at [wileyonlinelibrary.com](https://onlinelibrary.wiley.com/doi/10.1002/app.54035)]

was always at the gage section. Length between the center of two discs was taken as the gage length. Grooved discs were 3-D printed from PLA and were used for both

tensile and strain-hardening tests. A test set-up with PLA discs is shown in Figure 2. Tensile tests were conducted using a Zwick-Roell materials testing machine. A cross-head speed of 2.5 mm/min and a gage length of 15 mm were used for each test. This gave a strain rate of $2.77 \times 10^{-3} \text{ s}^{-1}$. A 20 N load cell with 1 mN accuracy was used. Tests were conducted under displacement control mode. The diameter of the filament was measured prior to testing using a tabletop SEM.

3.2 | Strain hardening

Strain hardening tests were conducted in the same Zwick–Roell materials testing machine utilizing its cyclic module. Repeated loading and unloading promotes alignment of molecular segments and nanotubes along the axis of the fiber. Functional groups present at nanotube surface further enforced alignment of nanotubes along with chain molecules. Strain hardening began by setting initial load at 0.1 N with an increment of 0.02 N for each cycle. After each incremental loading, fiber was completely unloaded, and a new cycle would start. A sample loading–unloading hysteresis loops for SWCNT-ODA fiber during strain hardening are shown in Figure 3. Loading and unloading speed was 2.5 mm/min similar to that of quasi-static tensile tests. Identical sample size and fiber mounting procedures were followed. Strain hardening was performed for 15–20 cycles and then the fiber was loaded to failure as seen in Figure 3. It is noticed in Figure 3 that as strain hardening progressed, both stress and modulus of the fiber increased after each

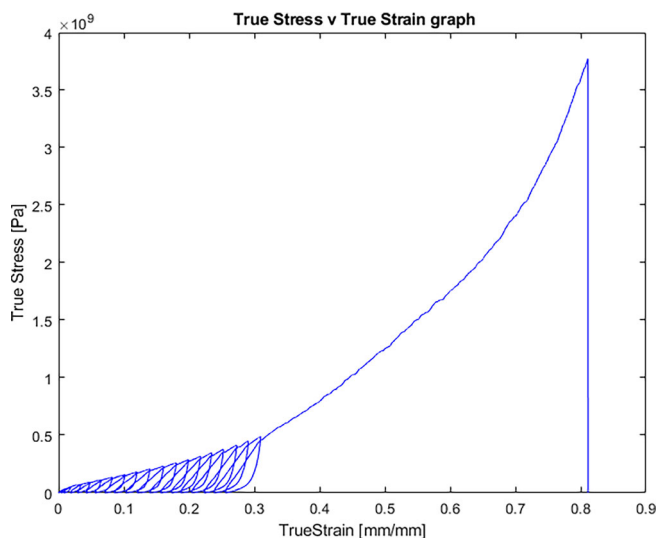


FIGURE 3 Sample stress–strain hysteresis loops during strain hardening of nanohybrid-SWCNT-ODA fiber. [Color figure can be viewed at wileyonlinelibrary.com]

cycle. After the last cycle, when the fiber was loaded to failure, stress increased significantly. The last cycle in the stress–strain diagram was used to calculate modulus, strength, and fracture strain. After several iterations the number of cycles (loops) for strain hardening was finalized that gave maximum gain in modulus and strength with a minimum reduction of the fracture strain.

4 | RESULTS AND DISCUSSION

4.1 | Tensile tests

Tensile testing of fiber was conducted before and after strain hardening to determine the effect of strain hardening on fiber properties. Sample stress–strain diagrams for three categories of fiber: neat UHMWPE, nanohybrid SWCNT-COOH, and nanohybrid SWCNT-ODA are shown in Figure 4. The results in Figure 4 are for fibers before strain hardening. Figure 4 reveals that neat UHMWPE sample has large plastic strain compared to nanohybrid samples. After UHMWPE was hybridized and reinforced with SWCNT-COOH or SWCNT-ODA, modulus, and strength increased sharply. It is also noticed that gain in modulus and strength is by sacrificing a significant amount of fracture strain. This was expected since embedded nanotubes without being fully stretched, restricted the elongation of UHMWPE macromolecules. Modulus, strength, and fracture strain measured from the curves were used in the calculation of normalizing velocity as shown in Equation (1). Densities

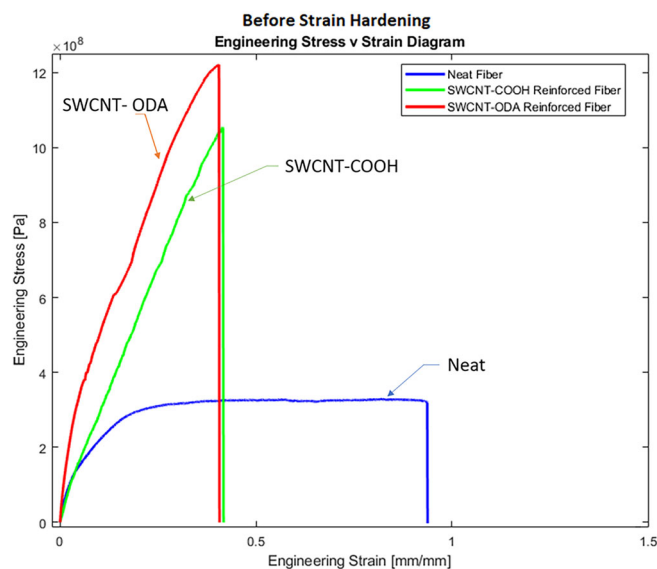


FIGURE 4 Stress–strain diagrams for three different fiber categories before strain hardening. [Color figure can be viewed at wileyonlinelibrary.com]

TABLE 2 Fiber properties before and after strain hardening.

Fiber Type	Modulus (GPa)		Ultimate strength (GPa)		Fracture strain (mm/mm)	Normalizing velocity (km/s)	
	Before/after	% Increase	Before/after	% Increase		Before/after	% Increase
Neat UHMWPE	2.2/3.76	71	0.4/0.48	20	0.94/0.58	0.67/0.79	18
Nanohybrid SWCNT-COOH	2.4/6.45	169	1.0/2.34	134	0.49/0.59	0.74/1.24	68
Nanohybrid SWCNT-ODA	5.6/13	132	1.2/2.78	132	0.52/0.47	0.87/1.27	46

TABLE 3 Mechanical properties of SWCNT-ODA and commercial fibers.

Fiber type	Modulus (GPa)	Ultimate strength (GPa)	Fracture strain (mm/mm)	Normalized velocity (km/s)
Nanohybrid SWCNT-ODA	13.0	2.78	0.47	1.27
Spectra-2000	116	3.25	0.029	0.81
Dyneema-SK75	107	3.4	0.038	0.88

of UHMWPE, nylon, and nanotubes were taken as 970, 1140, and 2260 kg/m³, respectively. For nanohybrid fiber, density was calculated using the rule of mixture and their concentrations.

Mechanical properties obtained from the tensile tests are presented in Table 2. Five to six samples were tested in each category and the average values are listed in the table. Table 2 also includes results after strain hardening. Modulus, strength, and fracture strain after strain hardening were obtained from the last loop of the hysteresis diagram shown in Figure 3. As observed in Figure 3, modulus and strength increase as the cycling continues. Percent change in properties due to strain hardening is also indicated in Table 2. It is clear in Table 2 that in case of nanohybrids, the increase in modulus and strength is more pronounced. For example, with SWCNT-COOH fiber, increase in modulus and strength is 169% and 134%, respectively after strain hardening. The trend is similar with SWCNT-ODA fiber. However, with neat UHMWPE, the increase in modulus and strength is only 71% and 20% after strain hardening. This suggests that the effect of strain hardening is more pronounced in nanohybrids than in neat UHMWPE. Structural changes in nanohybrids caused by hybridization and nanotube reinforcement are responsible for this behavior.

The normalizing velocity is highly influenced by strain hardening as seen in Table 2. It is observed that the highest normalizing velocity is given by nanohybrid SWCNT-ODA fiber. Mechanical properties of nanohybrid SWCNT-ODA fiber with those of Dyneema SK-75 and Spectra-2000 are listed in Table 3. It is observed that nanohybrid fiber has one order lower modulus, but one

order higher fracture strain than Dyneema and Spectra fibers. Ultimate strength of nanohybrids is of the same order. The resulting normalizing velocity of nanohybrid SWCNT-ODA fiber is 1270 m/s which is about 50% higher than that of Spectra-2000 and Dyneema SK-75.

4.2 | Differential scanning calorimetry

DSC analysis of neat UHMWPE and different categories of nanohybrid fibers was performed to investigate thermal and morphological changes in polymer due to hybridization and nanotube reinforcement. In addition to the fibers listed in Table 2, two more categories were included in the DSC analysis; one was hybridized UHMWPE with nylon (i.e., 80% UHMWPE and 20% nylon) and the other was nanohybrid fiber reinforced with SWCNT without any functionalization. Sample weight was 5 mg. DSC curves for neat UHMWPE and nanohybrid SWCNT-ODA fibers are shown in Figures 5 and 6. Data reduced from all DSC curves are presented in Table 4. The table shows melting peak, area under the melting endotherm, crystallization onset (T_o), and peak (T_p) temperatures extracted from DSC curves.

Melting peaks and melting endotherms shown in Figures 5 and 6 are distinct since melting is a first-order thermodynamic transition. The melting temperatures of neat UHMWPE and nanohybrid-SWCNT-ODA fibers are close, about 130°C as seen in Table 4. This is in agreement with other researchers.^{30–32} However, it is observed in Table 4 that when UHMWPE is hybridized with nylon (without any reinforcement of nanotubes), the melting

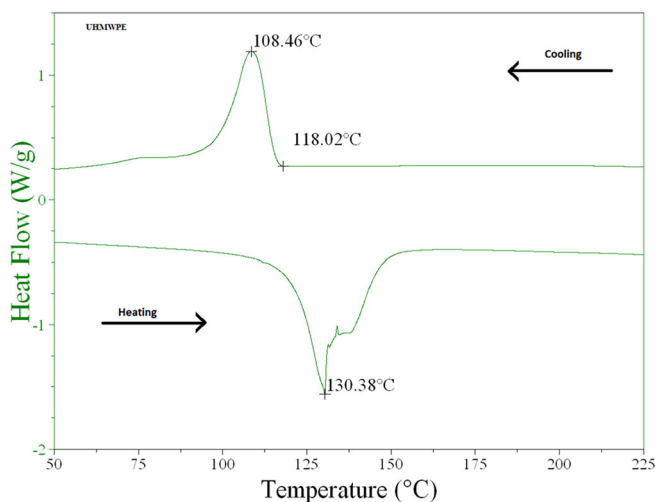


FIGURE 5 DSC heating and cooling curves for neat UHMWPE fiber. [Color figure can be viewed at wileyonlinelibrary.com]

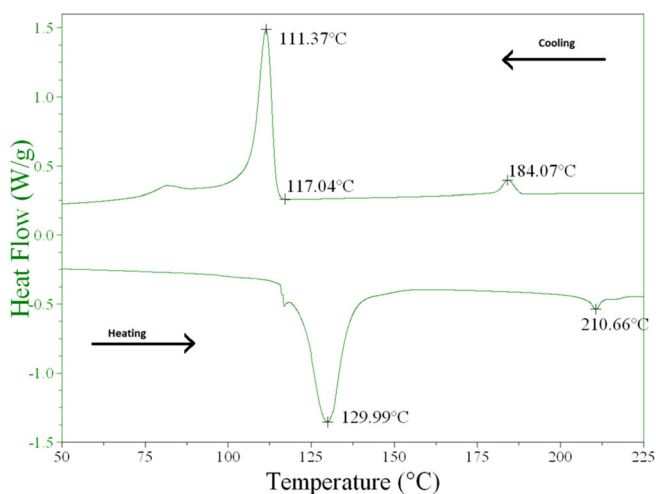


FIGURE 6 DSC heating and cooling curves for SWCNT-ODA reinforced fiber. [Color figure can be viewed at wileyonlinelibrary.com]

TABLE 4 DSC results for neat UHMWPE and nanohybrid fibers.

Fiber type	Melting peak (°C)	Area under melting endotherm (J/g)	Crystallinity (%)	Crystallization onset (T_o) (°C)	Crystallization peak (T_p) (°C)	($T_o - T_p$) (°C)
Neat UHMWPE	130	138	47	118	108	10
Hybridized UHMWPE with nylon	133	98	34	121	114	7
Nanohybrid SWCNT	129	120	41	121	113	8
Nanohybrid SWCNT-COOH	130	68	23	117	114	3
Nanohybrid SWCNT-ODA	129	75	26	117	111	6

peak increases to 133°C. This slight shift to higher temperature is due to the reason that nylon has a higher melting temperature than UHMWPE. It therefore appears that while hybridization increases the melting temperature slightly, nanotube reinforcement brings it back to 130°C as seen in Table 4. A different scenario is observed when we consider the area under the melting endotherm. Crystallinity is calculated from this area dividing it by melting enthalpy of 100% crystalline UHMWPE (~293 J/g). It is observed that the area reduced significantly with nanohybrid samples. Table 3 shows that area for neat UHMWPE is 138 J/g while those for SWCNT-COOH and SWCNT-ODA are 68 and 75 J/g, respectively. When nanotubes are not functionalized, i.e., with nanohybrid SWCNT, the area is 120 J/g. This suggests that functionalization of nanotubes helps reduce melting enthalpy. Decrease in melting enthalpy is associated with the loosening of UHMWPE structures caused by interaction between polymer and functionalized nanotubes. Due to the interaction, the functionalized surface of nanotubes can act as nucleating agents inducing morphological changes. Ordering of polymer molecules into crystals is disrupted by such nucleation which affects crystallinity of the polymer. When UHMWPE is only hybridized, or nanotubes are not functionalized, such nucleation is less. The result is evident in Table 4. Crystallinity of neat UHMWPE is 47% while it is 41% and 34% for hybridized and nanohybrid-SWCNT samples. However, crystallinity reduces drastically to 23% and 26% for SWCNT-COOH and SWCNT-ODA samples that are almost half of neat UHMWPE. It is clear that addition of nylon and functionalized nanotube fillers contribute to the reduction in crystallinity.

As seen in Figures 5 and 6, it was not possible to capture the crystallization temperature during the heating cycle. However, the cooling cycle reveals a crystallization peak. Crystallization onset (T_o) and peak (T_p) temperatures were extracted from DSC curves and are listed in

Table 4. It is observed that there is a decrease in ($T_o - T_p$) values from 10 and 7 for neat UHMWPE and hybridized samples to 3 and 6 for nanohybrid samples. The trend is similar with percent crystallinity. This was expected and further proves lamellar structural changes in UHMWPE due to hybridization and nanotube reinforcement. In the DSC curve of Figure 6 (SWCNT-ODA), two additional peaks are observed at around 210°C and 184°C. The peak at 210°C is observed during the heating cycle and is endothermic. It is above the melting point of UHMWPE (130°C) and represents melting of nylon. Although the melting temperature of nylon is about 220°C, the value (210°C) obtained here is slightly less due to hybridization and nanotube reinforcement. An exothermic peak is observed at 184°C in Figure 6 during cooling. This represents the crystallization temperature of nylon. These two peaks together suggest that even after hybridization and nanotube reinforcement, nylon phase remains intact and nanohybrid fiber remains as a two-phase polymer system.³³ Each phase maintains its individual melting and crystallization peaks, but crystallization morphology alters significantly.

4.3 | Raman spectroscopy

The purpose of Raman spectroscopy was to investigate mechanical deformation of nanotubes and to evaluate interaction between embedded nanotubes and the surrounding polymer by using Raman band shifts. As nanohybrid fibers are subjected to tension, nanotubes undergo longitudinal and lateral strains which can be detected by a shift in Raman band at a particular frequency. The spectra shown in Figure 7 reveal peaks corresponding to molecular vibrations at various wave numbers. Peaks at 1058 and 1123 cm^{-1} frequency correspond to C—C asymmetric and symmetric stretching modes of polyethylene (PE). Since PE is present in both cases, two peaks are at identical frequencies. CH_2 wagging mode of PE is also evident at 1292 cm^{-1} frequency in both cases. The orthorhombic crystalline phase of PE is noticed at 1414 cm^{-1} peak. This orthorhombic phase is the secondary phase of crystallization as PE crystallizes from the primary hexagonal phase. This peak is only observed with the SWCNT-ODA sample indicating that reinforcement of nanotubes has caused this change in the crystalline structure of UHMWPE. In addition, two more peaks at 1328 and 1585 cm^{-1} are visible in Figure 7. The strong Raman band (sharp peak with high intensity) at 1585 cm^{-1} is the characteristic G band and is due to the presence of nanotubes. G-band is not visible with the neat sample in Figure 7. The G-band appearing at 1585 cm^{-1} represents the graphene in-plane sp^2 vibrational mode. When a

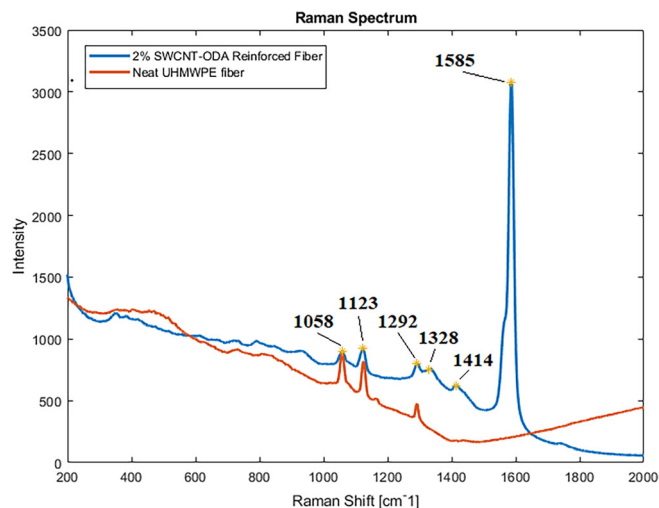


FIGURE 7 Raman spectra of Neat UHMWPE and SWCNT-ODA reinforced hybrid fiber. [Color figure can be viewed at wileyonlinelibrary.com]

graphene sheet is rolled to form a nanotube, the sp^2 hybrid orbital is deformed for rehybridization toward sp^3 orbital or σ — π bond mixing in nanotubes.^{34,35} G-band peak therefore confirms the presence of nanotubes in SWCNT-ODA fiber. The minor peak at 1328 cm^{-1} is attributed to D-band which arises due to structural disorder in nanotubes and is evident in nanohybrid SWCNT-ODA sample shown in Figure 7.³⁶

Raman spectroscopy of nanohybrid SWCNT-ODA samples before (i.e., pristine) and after strain hardening are shown in Figure 8. The G- and D-band peaks are visible but there is a frequency shift between the pristine and strain hardened samples. The G-band characteristic is due to the curvature and confinement of graphene layers in forming the nanotubes as mentioned earlier. On the other hand, the D-band is activated due to the first-order scattering process of sp^2 carbons. We particularly focused on G- (1585 cm^{-1}) and D- (1330 cm^{-1}) band frequency shift due to strain hardening. It is noticed in Figure 8 that the G-band peak had shifted from 1585 cm^{-1} to 1581 cm^{-1} due to strain hardening. This negative shift indicates stretching of C-C bonds meaning an elongation of SWCNT due to repeated loading and unloading. On the other hand, a slight positive shift in D-band peak from 1330 to 1332 cm^{-1} is observed in Figure 8. Such a positive shift is indicative of lateral compression of CNTs.^{37,38} Collectively these two shifts demonstrate that during strain hardening, nanotubes are stretched and laterally compressed. Such deformation feature of nanotubes establishes that they carry load during strain hardening and co-continuously deform with UHMWPE fibrils to enhance the modulus and strength of the nanohybrid fiber.

4.4 | SEM examination

SEM examination of neat UHMWPE and hybridized SWCNT-ODA fibers was conducted to study the role of nylon and nanotubes in fiber performance. Prior to extrusion, both UHMWPE and nylon powders are dissolved in paraffin oil and the admixture is heated in the extruder to form gels. In this process, nylon forms into microspheres (droplets), remains embedded within UHMWPE fibrils, and gets slightly elongated during extrusion. Embedded nylon microspheres within the long UHMWPE ligaments are seen in the SEM micrograph of Figure 9a. Our fiber was extruded at 135°C which is far below the melting point of nylon (210°C) meaning that microspheres remained solid within the UHMWPE fibrils

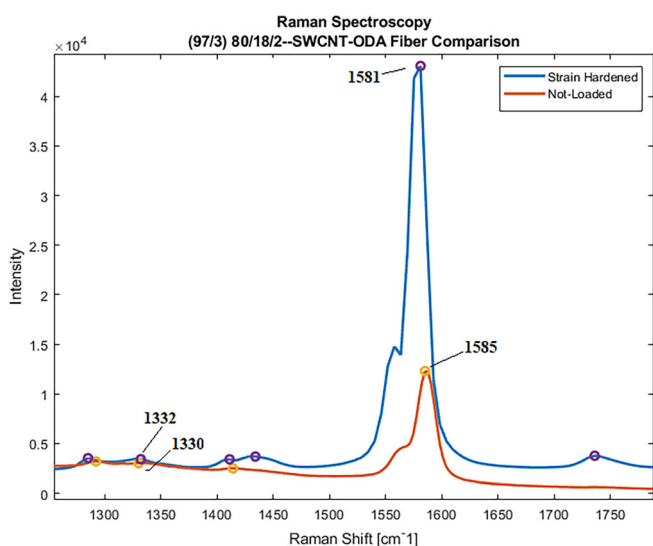


FIGURE 8 Raman spectra of pristine (not loaded) and strain-hardened SWCNT-ODA fiber. [Color figure can be viewed at [wileyonlinelibrary.com](https://onlinelibrary.wiley.com)]

after extrusion. Solid and elongated nylon microspheres are visible in Figure 9a,b. Axially elongated polyethylene ligaments are also visible along the extrusion direction. Polymer chain alignment observed in Figure 9a is due to extrusion and heat-stretching. After strain hardening, polymer chains are distorted as observed in Figure 9b. This is due to repeated loading and unloading. Nylon microspheres are still intact and embedded between PE ligaments (Figure 9b). The presence of nylon microspheres in the fiber facilitates disentanglement of large UHMWPE molecular chains and promotes sliding between crystalline lamella during tensile loading allowing large fracture strain. To further investigate the alignment of nanotubes after strain hardening, SWCNT-ODA fibers were examined under FE-SEM as shown in

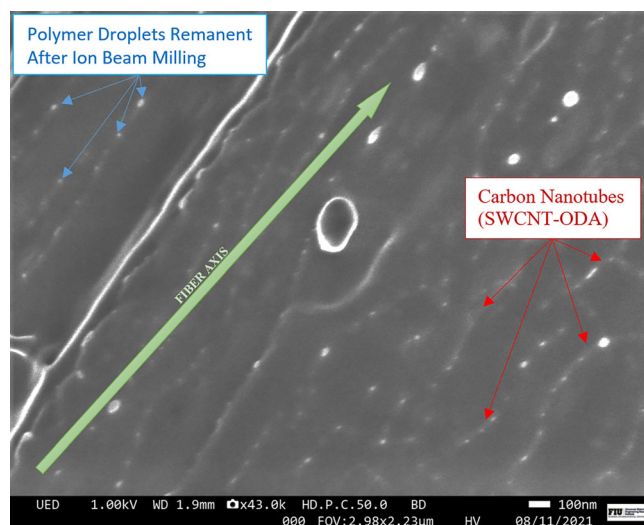


FIGURE 10 FE-SEM image of SWCNT-ODA fiber showing nanotube alignment. [Color figure can be viewed at [wileyonlinelibrary.com](https://onlinelibrary.wiley.com)]

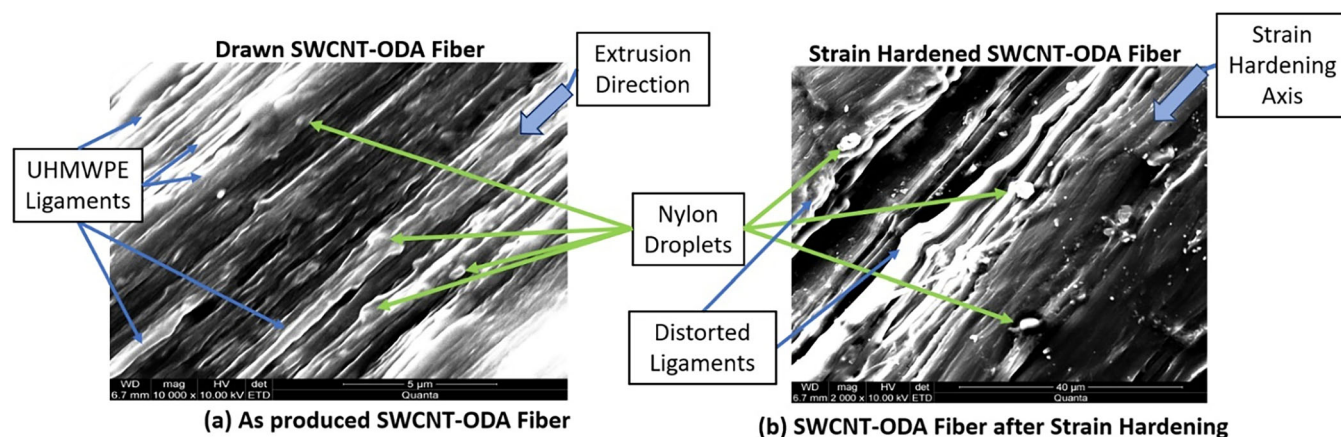


FIGURE 9 SEM Micrographs of SWCNT-ODA fiber before and after strain hardening. [Color figure can be viewed at [wileyonlinelibrary.com](https://onlinelibrary.wiley.com)]

Figure 10. The fiber surface was prepared by Gallium ion milling to expose the nanotubes embedded within the polymer. Figure 10 shows polymer remnants attached to nanotubes after milling. It is observed in Figure 10 that CNTs are aligned along the axis of the fiber and are well dispersed.

5 | CONCLUSION

This investigation shows a pathway to modify the structure of UHMWPE by hybridizing it with nylon and reinforcing with carbon nanotubes (CNT) to produce high-performance ballistic fibers. Hybridization and nanotube reinforcement techniques are simple and well within the realm of regular fiber spinning process. Given the limitations of a laboratory scale extruder and heat-stretching capability, the diameter of as-produced fiber was between 20 and 50 μm which is slightly higher than 18 μm of commercial Dyneema fiber. Two types of functionalized nanotubes; SWCNT-COOH and SWCNT-ODA were used in the study and the latter category gave the best performance with respect to normalizing velocity.

A comprehensive fiber testing plan was implemented by using 3-D printed PLA discs to avoid slippage in the grips and to have failure at the gage section. Strain hardening of fibers was performed using the same PLA discs. Tensile tests of strain-hardened fiber revealed that compared to commercial ballistic fibers, the nanohybrid fiber has one order of magnitude lower modulus, similar strength but one order of magnitude higher fracture strain. The resulting normalizing velocity of strain-hardened SWCNT-ODA fiber was 1270 m/s which exceeds Spectra-2000 (809 m/s) and Dyneema-SK75 (887 m/s) by 44%–57%.

DSC studies show that both UHMWPE and nylon remain phase-separated in the nanohybrid fiber. Each phase retains their respective melting behavior but their crystallinity changes. Crystallinity for two nanohybrid fibers reduced to 23% and 26%. Although the reduction in crystallinity is counterintuitive to increase in modulus and strength, the effect is compensated by sharing of load by nanotubes. Raman spectroscopy demonstrated that embedded nanotubes undergo permanent elongation and lateral compression during axial loading of fiber. This implies that nanotubes contribute to load sharing with UHMWE ligaments. SEM examination confirms alignment of nanotubes along the fiber axis providing further evidence of load-sharing. Micrographs also show the presence of nylon microspheres as a separate phase embedded within the UHMPE fibrils. Thus, structural changes induced by hybridization and nanotube reinforcement coupled with strain hardening result in higher normalizing velocity.

AUTHOR CONTRIBUTIONS

Hassan Mahfuz: Conceptualization (lead); project administration (lead); writing – original draft (lead); writing – review and editing (lead). **Leif Carlsson:** Formal analysis (equal); project administration (equal); writing – original draft (supporting); writing – review and editing (equal). **Oren Masory:** Formal analysis (equal); methodology (equal); project administration (equal); writing – review and editing (supporting). **Tye Langston:** Conceptualization (equal); investigation (equal); writing – review and editing (supporting). **Vitor Prado Correia:** Data curation (lead); formal analysis (equal); investigation (supporting); methodology (equal). **Tristan Irons:** Data curation (supporting); formal analysis (supporting); methodology (equal).

ACKNOWLEDGMENTS

The authors would like to thank Irregular Warfare Technical Support Directorate (IWTSD) for supporting this research through Contract Number: N4175619C3083.

DATA AVAILABILITY STATEMENT

Data included in the paper is for public release.

ORCID

Hassan Mahfuz  <https://orcid.org/0000-0002-1966-526X>

REFERENCES

- [1] B. P. Russell, K. Karthikeyan, V. S. Deshpande, N. A. Fleck, *Int. J. Impact Eng.* **2013**, *60*, 1.
- [2] S. L. Phoenix, P. K. Porwal, *Int. J. Solids Struct.* **2003**, *40*, 6723.
- [3] M. Khan, H. Mahfuz, T. Leventouri, *J. Mater. Res.* **2012**, *27*, 2657.
- [4] G. R. Hatfield, J. H. Glans, W. B. Hammond, *Macromolecules* **1990**, *23*, 1654.
- [5] D. R. Holmes, C. W. Bunn, D. J. Smith, *J. Polym. Sci.* **1955**, *17*, 159.
- [6] H. Arimoto, M. Ishibashi, M. Hirai, Y. Chatani, *J. Polym. Sci. Part A* **1965**, *3*, 317.
- [7] H. Mahfuz, M. Hasan, V. Rangari, S. Jeelani, *Macromol. Mater. Eng.* **2007**, *292*, 437.
- [8] H. Mahfuz, M. Hasan, V. Dhanak, G. Beamson, J. Stewart, V. Rangari, X. Wei, V. Khabashesku, S. Jeelani, *Nanotechnology* **2008**, *19*, 445702.
- [9] H. Mahfuz, A. Adnan, V. K. Rangari, M. M. Hasan, S. Jeelani, W. J. Wright, S. J. DeTeresa, *Appl. Phys. Lett.* **2006**, *88*, 083119.
- [10] L. Jin, C. Bower, O. Zhou, *Appl. Phys. Lett.* **1998**, *73*, 1197.
- [11] C. A. Cooper, D. Ravich, D. Lips, J. Mayer, H. D. Wagner, *Compos. Sci. Technol.* **2002**, *62*, 1105.
- [12] A. B. Sulong, J. Park, *J. Compos. Mater.* **2011**, *45*, 931.
- [13] E. T. Thostenson, T. W. Chou, *J. Phys. D. Appl. Phys.* **2002**, *35*, L77.
- [14] J. Gao, M. E. Itkis, A. Yu, E. Bekyarova, B. Zhao, R. C. Haddon, *J. Am. Chem. Soc.* **2005**, *127*, 3847.
- [15] M. R. Khan, H. Mahfuz, T. Leventouri, V. K. Rangari, A. Kyriacou, *Polym. Eng. Sci.* **2010**, *51*, 654. <https://doi.org/10.1002/pen.21873>

- [16] H. Mahfuz, M. R. Khan, T. Leventouri, *J. Nanotechnol.* **2011**, 2011, 1.
- [17] M. R. Khan, H. Mahfuz, T. Leventouri, A. Adnan, *J. Mater. Eng. Perform.* **2013**, 22, 1593.
- [18] M. R. Khan, H. Mahfuz, A. Adnan, *Fibers Polym.* **2014**, 15, 1484.
- [19] M. R. Khan, S. Absar, H. Mahfuz, K. Edwards, *Polym. Sci.* **2015**, 57, 863.
- [20] S. Hulsey, S. Absar, Q. Nahida, S. Sabet, H. Mahfuz, M. Khan, *Polym. Compos.* **2017**, 39, e1025. <https://doi.org/10.1002/pc.24444>
- [21] B. R. C. De Menezes, F. V. Ferreira, B. C. Silva, E. A. N. Simonetti, T. M. Bastos, L. S. Cividanes, G. P. Thim, *J. Mater. Sci.* **2018**, 53, 14311.
- [22] T. Lyashenko-Miller, G. Marom, *Polym. Adv. Technol.* **2017**, 28, 606.
- [23] R. Chen, C. Ye, Z. Xin, J. Zhao, X. Meng, *J. Polym. Res.* **2018**, 25, 135.
- [24] Y. Wang, J. Fu, J. Yu, Q. Song, J. Zhu, Y. Wang, Z. Hu, *Adv. Fiber Mater.* **2022**, 4, 280.
- [25] Y. Wang, J. Fu, Q. Song, J. Yu, Y. Wang, *J. Appl. Polym. Sci.* **2022**, 139, e52653.
- [26] H. Yuan, C. Long, J. Yu, F. Ke, T. Shiono, Z. Cai, *Adv. Fiber Mater.* **2022**, 4, 786.
- [27] ASTM C1557-20. "Standard Test Method for Tensile Strength and Young's Modulus of Fibers," ASTM International, 100 Barr Harbor Drive, West Conshohocken, PA 19428-2959, USA.
- [28] B. Sanborn, A. M. DiLeonardi, T. Weerasooriya, *J. Dyn. Behav. Mater.* **2015**, 1, 4.
- [29] J. H. Kim, N. A. Heckert, S. D. Leigh, H. Kobayashi, W. G. McDonough, K. D. Rice, G. A. Holmes, *J. Mater. Sci.* **2013**, 48, 3623.
- [30] S. H. Yetgin, *J. Mater. Res. Technol.* **2019**, 8, 4725.
- [31] K. Beate, B. Regine, H. Liane, P. Petra, *Compos. Sci. Technol.* **2015**, 114, 119.
- [32] M. Hasan, Y. Zhou, H. Mahfuz, S. Jeelani, *Mater. Sci. Eng. A* **2006**, 429, 181.
- [33] E. Parodi, L. E. Govaert, G. W. M. Peters, *Thermochim. Acta* **2017**, 657, 110.
- [34] R. P. Vidano, D. B. Fishback, L. J. Willis, T. M. Loehr, *Solid State Commun.* **1981**, 39, 341.
- [35] C. Thomsen, S. Reich, *Phys. Rev. Lett.* **2000**, 85, 5214.
- [36] S. D. M. Brown, A. Jorio, M. S. Dresselhaus, and G. Dresselhaus, *Phys. Rev. B*, **2001**, 64, 073403.
- [37] M. Mu, S. Osswald, Y. Gogotsi, K. Winey, *Nanotechnology* **2009**, 20, 335703.
- [38] L. S. Schadler, S. C. Giannaris, P. M. Ajyan, *Appl. Phys. Lett.* **1998**, 73, 3842.

How to cite this article: H. Mahfuz, L. A. Carlsson, O. Masory, T. Langston, V. P. Correia, T. Irons, *J. Appl. Polym. Sci.* **2023**, e54035. <https://doi.org/10.1002/app.54035>